LES of the Ranque-Hilsch Vortex Tube

W.R. Michałek, J.G.M. Kuerten, J.C.H. Zeegers and R. Liew

1 Introduction

The Ranque-Hilsch vortex tube (RHVT) is a device without any moving parts in which pressurized inlet gas is separated into a hot peripheral and a cold inner stream [1]. The RHVT is commonly used in industry although the nature of the energy separation is not well understood.

The first theories for the energy separation were published shortly after the invention of the RHVT [2–5]. The secondary circulation inside the RHVT was mentioned in several publications [2, 6]. Ahlborn et al. [7] proposed a closed loop system and suggested a heat pump mechanism transferring energy in the RHVT. Liew et al. measured wobbling [8] of the vortex and proposed a new theory [9] for the mechanism of energy separation and a model that matches the measurements well. Many numerical investigations on the RHVT were conducted in two- and three-dimensional domains. Only Kazantseva et al. [10] reported precession of the axial vortex.

The high swirl conditions of the flow in the RHVT allow us to expect good capabilities for droplet separation. The expansion of the tangentially introduced gas in the vortex chamber leads to a temperature drop and condensation of droplets. The gas acceleration and a large swirl cause the movement of droplets towards the wall. Thus, the main goals of this research are the investigation and improvement of the separation rate by droplet-laden large-eddy simulation (LES) of the RHVT utilizing ANSYS FLUENT. The results of the LES will be validated by comparison with the results of laser Doppler anemometry (LDA) measurements of particle velocity, concentration and size in the RHVT.

W.R. Michałek (✉) · J.G.M. Kuerten
Department of Mechanical Engineering,
Eindhoven University of Technology, Eindhoven, The Netherlands
e-mail: w.michalek@tue.nl

J.C.H. Zeegers · R. Liew
Department of Applied Physics, Eindhoven University of Technology,
Eindhoven, The Netherlands

J. Fröhlich et al. (eds.), *Direct and Large-Eddy Simulation IX*,
ERCOFTAC Series 20, DOI 10.1007/978-3-319-14448-1_85

2 Equations, Numerical Methods, Mesh and Setup

The Euler-Lagrange approach was used to solve the particle-laden flow. For the fluid, the momentum, energy and the continuity equation are solved. The trajectories of particles are solved by integration of the particle equation of motion, $\frac{d\mathbf{u}}{dt} = F_D(\mathbf{u}-\mathbf{v})$, where $F_D(\mathbf{u}-\mathbf{v})$ is the drag force per unit particle mass with $\mathbf{v}$ the particle velocity, $\mathbf{u}$ the fluid velocity at the particle position, and $F_D = 3\mu C_D Re/4\rho_p d_p^2$, with μ the molecular viscosity of the fluid, ρ_p the particle mass density, d_p the particle diameter, $\mathrm{Re}_p = \rho d_p|\mathbf{v}-\mathbf{u}|/\mu$ the relative Reynolds number with ρ the fluid mass density and C_D is the drag coefficient.

In order to avoid too large restrictions on the time step, the coupled pressure-based solver was chosen for the RHVT flow simulation. This is possible since there are no shocks in the flow. The second-order accurate bounded central-differencing method was used as the discretization scheme for the momentum equations. A second-order method is used to interpolate the pressure at the cell faces. The least squares cell-based method was chosen to calculate gradients and derivatives. The second-order upwind scheme is used to estimate the values of density and energy at cell faces, and a second-order implicit method for integration in time.

The geometry of the RHVT is presented in Fig. 1 and is similar to the one in the experiment. The domain contains a vortex chamber with eight tangential inlet slots. The diameters of the vortex tube and the vortex chamber are equal to 20 and 40 mm respectively, the total length 500 mm. Two outlets are present on the opposite sides of the RHVT. The cold outlet diameter is equal to 15 mm and the hot outlet dimensions are: $r_{in} = 17$ and $r_{out} = 20$ mm.

Figure 2 shows the section of the mesh through the vortex chamber. Since $\delta r^+ > 30$ at the wall, standard wall functions are used. The total number of cells equals 3, 223, 596 and the number of cells in the tangential and radial directions are respectively 112 and 122.

The fluid inlet and outlet boundary conditions are presented in Table 1 and these values correspond to the values measured in the experiments. The mass flux is defined at the hot outlet and inlet and at the cold outlet only the pressure and backflow temperature, so the total mass in the system can vary in time. At the walls no-slip adiabatic conditions are applied.

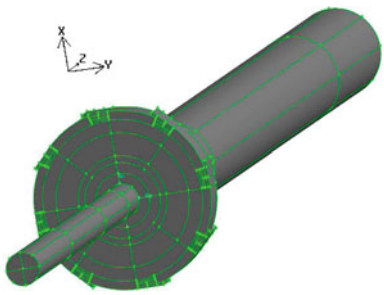

Fig. 1 Isometric view of the domain

Fig. 2 Computational grid

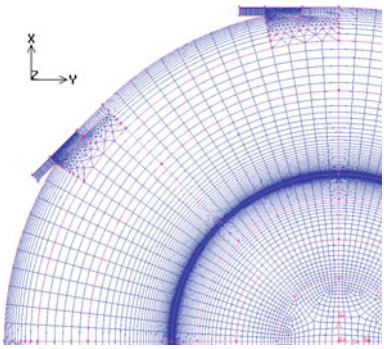

Table 1 Boundary conditions for a mass flow equal to 200 m_n^3/h

Type of boundary	Total pressure (bar)	Total temperature (K)	Mass flux (g/s)
Inlet	4.64	299	70.0
Hot outlet	1.82	319	45.5
Cold outlet	1.42	263	24.5

Particles with four diameters were injected ($d_p = 0.5$, 1, 1.5, and 2.5 μm) at 8 points each rotated by 45°. The injection point position is 0.1 mm from the inlet symmetry point. The initial particle velocity is equal to the mean fluid velocity at the injection point. At the walls, particles are trapped, at the outlets particles escape.

3 Fluid Results

A good agreement between experimental data by Liew et al. [8, 9] and results of the $k - \varepsilon$ turbulence model with the density-based solver can be seen in Fig. 3, where the Mach number is presented as a function of the radial coordinate at $z = 7$ mm (in the middle of the vortex chamber).

All results of the density-based solver are axially symmetric in the whole domain. This implies that the center of the vortex coincides with the axis. The final solution of the density based solver was used as the initial state for the pressure-based solver.

As can be seen in Fig. 4 the steady solution of the pressure-based solver is not axi-symmetric. This figure shows the mean tangential fluid velocity component as a function of the axial coordinate at three different locations for the two solvers. The center of the vortex does not coincide with the axis, especially in the range of axial coordinates between 100 and 300 mm and this implies wobbling of the vortex. Apart from the presence of oscillations, the swirl velocity is damped more strongly. The asymmetric character of the flow field disappears when in transient simulation.

The LES was started with the initial condition obtained with the $k - \varepsilon$ model and the coupled pressure-based solver. A steady state of turbulence was obtained after 30 ms. The time averaged quantities of the fluid were collected through 50 ms.

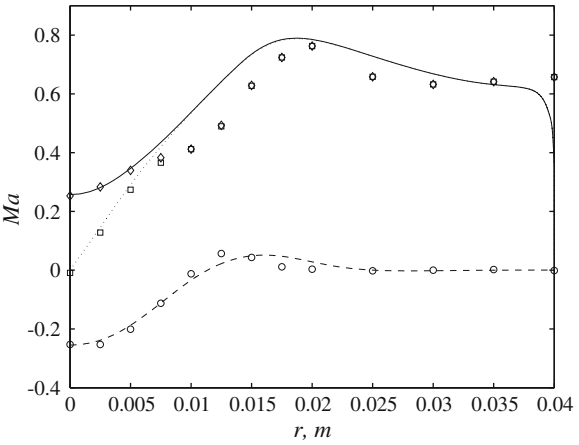

Fig. 3 Mach number as a function of the radial coordiate at $z = 7$ mm; *dashed* LES, axial component of the Mach number; *dotted* LES, tangential component of the Mach number; *solid* LES, total Mach number; *circles* experiment, axial component of the Mach number; *squares* experiment, tangential component of the Mach number; *diamonds* experiment, total Mach number

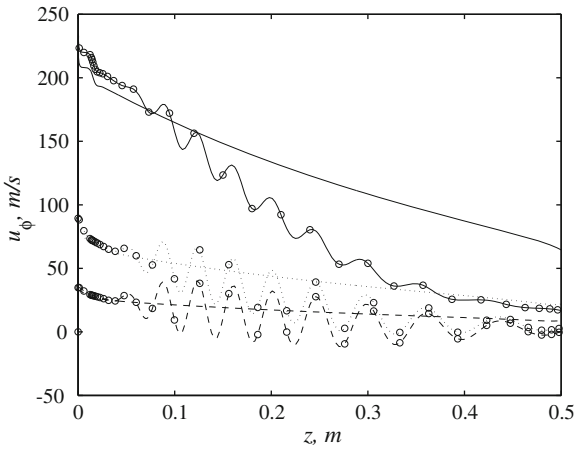

Fig. 4 Mean tangential fluid velocity as a function of the axial coordinate obtained with the $k - \varepsilon$ model at $y = 0$; *solid* $z = 16$ and $r = 0$ mm; *dotted* $r = 2$ mm; *dashed* $r = 5$ mm; *lines with circles* coupled pressure-based solver; *lines without circles* density based solver

Positive values of the axial fluid velocity are found in the peripheral area of the vortex tube and negative values in the core. A "camel hump" in the axial velocity profile (the maximum negative axial velocity is distanced from the axis) can be noticed, especially between $z = 200$ and $z = 350$ mm. Moreover, in the last 100 mm of the vortex tube the mean axial velocity equals zero. The presence of the stagnation point at the axis implies that a further elongation of the vortex tube will not increase the energy separation.

Figure 5 shows a contour plot of the mean tangential fluid velocity in a half cross section of the domain. In the vortex chamber between $r = 20$ and $r = 40$ mm a free vortex occurs. A forced vortex is present in the inner part of the vortex chamber and

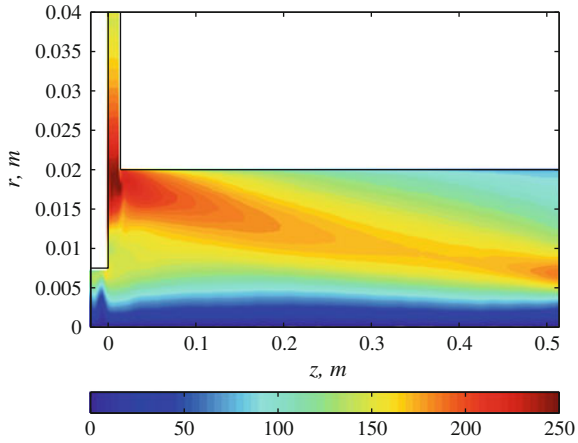

Fig. 5 Contour plot of the mean tangential fluid velocity [m/s] in a half cross section of the RHVT domain

in the beginning of the vortex tube (up to $z = 50$ mm). At further axial coordinates, the forced vortex is turning into a Rankine vortex due to the presence of the wall.

4 Particle Results

Particles were injected in the statistically steady state. A steady state of particle concentration was obtained after 20 ms. The particle time statistics were collected through the next 30 ms. The four sizes of particles considered allow us to investigate the behavior of different types of particles. The smallest particles considered are present along the whole length of the vortex tube. This can be seen in Fig. 6, where the decimal logarithm of the particle concentration is presented in a contour plot in a half cross section of the RHVT domain for $d_p = 0.5\,\mu$m. The second smallest

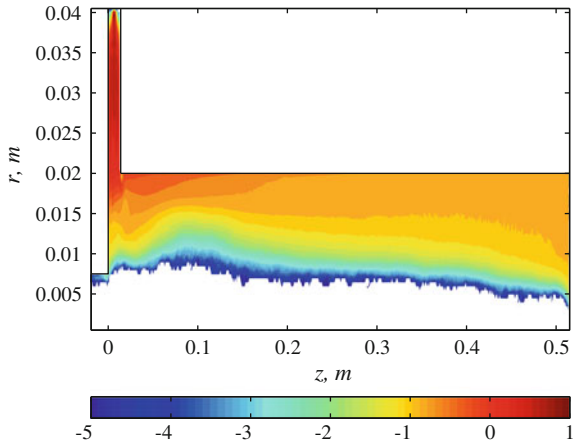

Fig. 6 Contour plot of the decimal logarithm of the particle concentration in a half cross section of the RHVT domain for $d_p = 0.5\,\mu$m

particles considered are also present in the whole length of the vortex tube, but the particle concentration after half of the tube length is very low. Particles with $d_p = 1.5\,\mu\text{m}$ are not present in the second half of the tube and with $d_p = 2.5\,\mu\text{m}$ are mainly present in the vortex chamber.

The smallest particles considered are good tracers while the largest particles are prevented to enter the vortex tube by the centrifugal force. The behavior of the particles can be characterized by their ability to migrate towards the wall. This can be visualized by the number of particles colliding with the wall per unit axial distance as a function of the axial coordinate and this is shown in Figs. 7 and 8 for the smallest and largest particles. The number of the smallest particles leaving the computational domain through the hot outlet is significant in comparison to the total amount of particles trapped at the wall. Some of the particles leave the domain through the cold outlet or are trapped at the cold outlet tube wall. The next larger particles behave in a similar way, but more particles are trapped by the wall. All particles

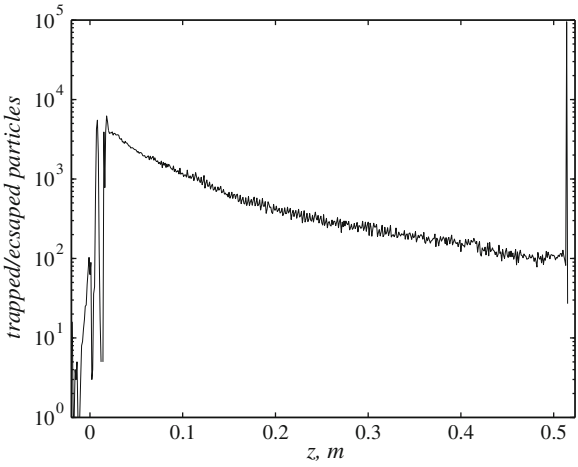

Fig. 7 Number of trapped/escaped particle per 1 mm as a function of the axial coordinate for $d_p = 0.5\,\mu\text{m}$

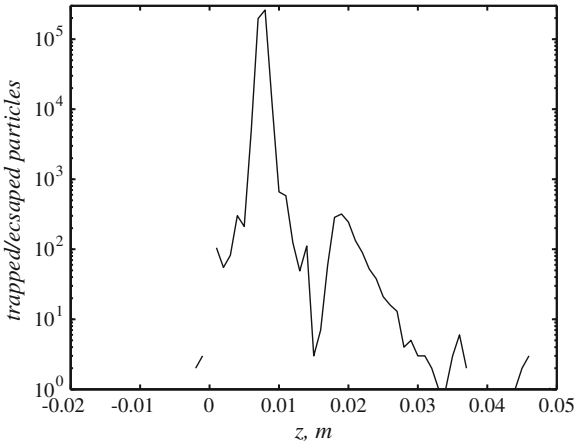

Fig. 8 Number of trapped/escaped particle per 1 mm as a function of the axial coordinate for $d_p = 2.5\,\mu\text{m}$

with $d_p = 1.5\,\mu\text{m}$ are collected at the wall of the vortex chamber or within the first 150 mm of the vortex tube. The vast majority of the largest particles considered is collected at the vortex chamber wall.

The mean axial and tangential particle velocity appear independent of particle size and is almost identical to the fluid velocity. In contrast, the mean radial particle velocity depends on the particle size. Figure 9 shows the mean radial particle velocity as a function of the radial coordinate at $z = 35$ mm. The profile of the mean radial particle velocity appears particle size independent for $r < 17\,\text{mm}$. From this radius outward, the mean radial velocity increases with the size of the particle due to the increasing effect of the centrifugal force. For all quantities except the axial velocity, the instantaneous result is similar to the time averaged result. However, the instantaneous axial velocity presented in Fig. 10 illustrates a non-uniformity in the axial direction which disappears after time averaging.

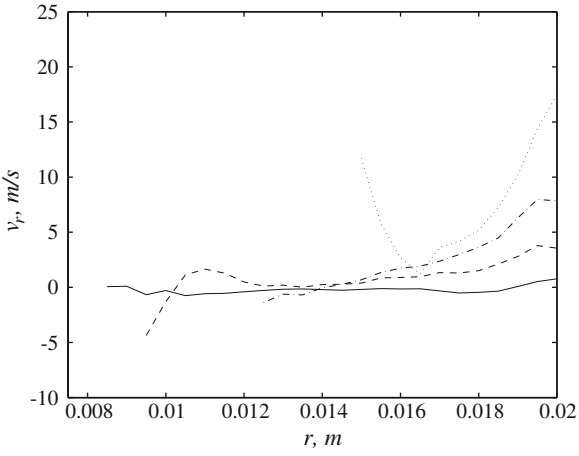

Fig. 9 Mean radial particle velocity as a function of the radial coordinate at $z = 35\,\text{mm}$; *solid* $d_p = 0.5\,\mu\text{m}$; *dashed* $d_p = 1.0\,\mu\text{m}$; *dashed-dotted* $d_p = 1.5\,\mu\text{m}$; *dotted* $d_p = 2.5\,\mu\text{m}$

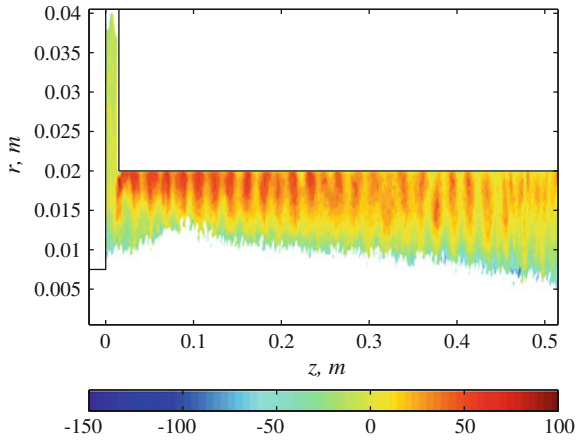

Fig. 10 Contour plot of the instantaneous axial particle velocity [m/s] in a half cross section of the RHVT domain for $d_p = 0.5\,\mu\text{m}$

5 Discussion

The good agreement in velocities between this numerical work and earlier performed experiments indicates that the fluid flow is properly solved in FLUENT. The particle-laden LES allows us to assess the capability of the RHVT as a particle separator. The RHVT is a particle separator for particles larger than 1.5 μm. The flow through the cold outlet has a much smaller particle concentration than the inflow. However, to investigate the real situation, the implementation of phase changes is crucial. Condensation is mainly present in the vortex chamber and in the beginning of the tube. Evaporation occurs in the rest of the vortex tube. Condensation enhances the separation and evaporation deteriorates the separation of the smaller particles. In future work evaporation and condensation models will be implemented.

Acknowledgments This research is supported by the Dutch Technology Foundation STW.

References

1. Ranque, G.J.: Methods and apparatus for obtaining from a fluid under pressure two outputs of fluid at different temperatures. U.S. Patent No. 1,952,281 (1934)
2. Fulton, C.D.: Ranque's tube. J. ARSE Refrig. Eng. *58*, 473–479 (1950)
3. Hilsch, R.: The use of expansion of gases in a centrifugal filed as a cooling process. Rev. Sci. Instrum. **18**(2), 108–113 (1947)
4. Kassner, R., Knoerschild, E.: Friction laws and energy transfer in circular flow. Wright-Patterson Air Force Base. Technical Report No. F-TR-2198-ND, Ohio (1948)
5. Kurosaka, M.: Acoustic streaming in swirling flow and the Ranque-Hilsch (vortex-tube) effect. J. Fluid Mech. **124**, 139–172 (1982)
6. Gao, C.M., Bosschaart, K.J., Zeegers, J.C.H., de Waele, A.T.A.M.: Experimental study on a simple Ranque-Hilsch vortex tube. Cryogenics **45**(3), 173 (2005)
7. Ahlborn, B., Keller, J.U., Rebhan, E.: The heat pump in a vortex tube. J. Non-Equilib. Thermodyn. **23**, 159–165 (1998)
8. Liew, R., Zeegers, J.C.H., Kuerten, J.G.M., Michałek, W.R.: 3D velocimetry and droplet sizing in the Ranque-Hilsch vortex tube. Exp. Fluids **54**, 1416 (2013)
9. Liew, R., Zeegers, J.C.H., Kuerten, J.G.M., Michałek, W.R.: Maxwell's demon in the Ranque-Hilsch vortex tube. Phys. Rev. Lett. **109**, 054503 (2012)
10. Kazantseva, O.V., Piralishvili, S.A., Fuzeeva, A.A.: Numerical simulation of swirling flows in vortex tubes. High Temp. **43**(4), 608–613 (2005)